Clim Dyn
DOI 10.1007/s00382-012-1553-3

Diagnostics of subseasonal prediction biases of the Asian summer monsoon by the NCEP climate forecast system

Xiangwen Liu · Song Yang · Arun Kumar · Scott Weaver · Xingwen Jiang

Received: 11 June 2012 / Accepted: 1 October 2012
© Springer-Verlag Berlin Heidelberg 2012

Abstract Biases of subseasonal prediction of the Asian summer monsoon are diagnosed using daily data from the hindcasts of 45-day integrations by the National Centers for Environmental Prediction Climate Forecast System version 2. The retrospective forecasts often show apparent systematic biases, which are mostly represented by the underestimation of the whole Asian monsoon. Biases depend not only on lead time, but also on the stage of monsoon evolution. An abrupt turning point of bias development appears around late June and early July, when ensemble spread and bias growth of winds and precipitation show a significant change over the northwestern Pacific (NWP) and the South Asian summer monsoon (SASM) region. The abrupt turning of bias development of winds, precipitation, and surface temperature is also captured by the first two modes of multivariate empirical orthogonal function analysis. Several features appear associated with the abrupt change in bias development: the western Pacific subtropical high (WPSH) begins its first northward jump and the surface temperature over the Tibetan Plateau commences a transition from warm bias to cold bias, and a reversal of surface temperature biases occurs in the eastern tropical Indian Ocean and the SASM region. The shift of WPSH position and the transition of surface thermal bias show close relationships with the formation of bias centers in winds and precipitation. The rapid growth in bias due to the strong internal atmospheric variability during short leads seems to mainly account for the weak WPSH and SASM in the model. However, at certain stages, particularly for longer-lead predictions, the biases of slowly varying components may also play an important role in bias development of winds and precipitation.

Keywords Subseasonal prediction biases · Short-lead predictions · Long-lead predictions · Western Pacific subtropical high · Asian summer monsoon

X. Liu
National Climate Center,
China Meteorological Administration,
Beijing, China

S. Yang (✉) · A. Kumar · S. Weaver
NOAA Climate Prediction Center,
5830 University Research Court, College Park,
MD 20740, USA
e-mail: Song.Yang@noaa.gov

X. Jiang
Institute of Plateau Meteorology, China Meteorological Administration, Chengdu, Sichuan, China

1 Introduction

The Asian summer monsoon (ASM) is the strongest monsoon system in the world and its variability is closely related to many prominent weather and climate phenomenon. It affects about half of the world's population and exerts strong socioeconomic influences on many countries, especially those in southern Asia. Given its robust impact on regional circulation and rainfall and its relationship with global climate systems (e.g., reviews in Wang 2006), prediction of ASM has been an important yet challenging task for both research and climate operations sectors.

Since statistical forecasts of the ASM are limited in skill (Gadgil et al. 2005) and show difficulty in providing spatial and temporal distributions of monsoon features, dynamical prediction has become a popular approach. For dynamical methods, improvements of Asian monsoon prediction can be linked to enhancements of model resolutions and initial

Published online: 16 October 2012

conditions (Sperber et al. 1994; Pope and Stratton 2002; Yang et al. 2008a; Wen et al. 2012), improvement of model physics (Yhang and Hong 2008; Yang et al. 2011), inclusion of air-sea coupling (Wang et al. 2005; Misra 2008), and application of multi-model ensemble methods (Kang et al. 2002; Wang et al. 2004; Krishnamurti et al. 2006), among others. In recent decades, assessing skill of dynamical prediction of the ASM has become an important subject in the academic community and many operational forecasting groups.

Nevertheless, significant difficulties remain in dynamical prediction of the ASM. In the absence of monsoon-ocean interaction, predictions of monsoon rainfall by atmosphere-alone models forced by observed sea surface temperature are not skillful except during El Niño and La Niña periods (Sperber and Palmer 1996; Wang et al. 2004, 2005). State-of-the-art climate models that fully take into consideration of the atmosphere–ocean–land coupled process are able to capture the primary modes of interannual variability of the Asian monsoon, but they underestimate the variances of monsoon variability (Wang et al. 2008). Moreover, while the large-scale monsoon features related to the impact of El Niño–Southern Oscillation (ENSO) are relatively predictable, predictions of regional features often show little skill (Yang et al. 2008a; Drbohlav and Krishnamurthy 2010).

In addition, models show limited skill in simulation and prediction of the subseasonal variability of ASM (Lin et al. 2008; Yang et al. 2008b; Achuthavarier and Krishnamurthy 2010). Monsoon intraseasonal oscillation, one of the typical phenomenons on subseasonal scale, is known as the apparent active-break cycles during monsoon season. The origin and northward propagation of the oscillation are closely related to the atmospheric internal dynamics involving feedback between convection and atmospheric dynamics (Jiang et al. 2004; Abhik et al. 2012) and complex ocean–atmosphere interaction (Sengupta et al. 2001; Fu et al. 2007). The predictability of monsoon intraseasonal oscillation is limited by its high sensitivity to both initial condition and underlying boundary condition (Krishnamurti et al. 1992). Meanwhile, monsoon intraseasonal oscillation is regarded as a barrier to high seasonal predictability (Goswami et al. 2006) due to its important modulation on the seasonal characteristics of monsoon rainfall (Hoyos and Webster 2007; Krishnamurthy and Shukla 2008). Nevertheless, several studies have revealed encouraging features about enhancement of intraseasonal prediction skill by improving model physics (Bechtold et al. 2008; Weaver et al. 2011) and initial conditions (Fu et al. 2009, 2011), or including air–sea coupling (Fu et al. 2007; Wang et al. 2009).

Difficulties in predicting the ASM are partially a result of the models' inability to reproduce the observed climatological mean state, which is an important factor that can limit prediction skill. Sperber and Palmer (1996) indicated that the accurate mean state is advantageous for models to capture the interannual variability of tropical precipitation correctly. Lau and Nath (2000) and Turner et al. (2005) showed that improvement of climatological mean state simulation can result in realistic simulation of ENSO-monsoon relationship. Lee et al. (2010) also pointed out that seasonal prediction skill of precipitation has a significantly positive correlation with the model's representation of the mean state. So although coupled models are expected to be suitable tools for monsoon prediction because of inclusion of air–sea interaction processes (Wang et al. 2003, 2005; Wu and Kirtman 2005), they often show deficiencies in reproducing realistic climatology due to model biases, which may actually lead to limiting their predictive capability. Previous studies have demonstrated that the coupled models that have a bias-corrected component could produce a more realistic internal variability and improved forecast skill (Chen et al. 2000; Barreiro and Chang 2004). Therefore, to improve the skill of predictions of the ASM by coupled dynamical forecast systems, it is necessary to have a better understanding of the systematic biases of models to move toward their correction.

The National Centers for Environmental Prediction (NCEP) Climate Forecast System (CFS), one of the state-of-the-art climate models, is an operational dynamical seasonal prediction system. The availability of comprehensive retrospective forecasts from the CFS offers an opportunity to understand the predictability of monsoon. Previous studies have demonstrated that the CFS is able to predict ASM with certain degree of skill (Yang et al. 2008a, b, 2011; Liang et al. 2009; Drbohlav and Krishnamurthy 2010; Lee et al. 2011; Wen et al. 2012). In this study, we diagnose the biases of ASM prediction by the CFS on subseasonal scale. We conduct several analyses to address the following questions. What, when, and where are the conspicuous biases in the subseasonal prediction of ASM? How are the biases in different fields linked to each other? How different are the biases during the different stages of monsoon evolution and as a function of lead time? What are the possible physical causes of the biases?

In Sect. 2, a brief overview of model and data is provided. In Sects. 3–6, we discuss the predictions of monthly climatological features, subseasonal evolution of tropical winds and rainfall, subseasonal variation of spread and errors, and the possible causes of biases, respectively. Summary and discussions are given in Sect. 7.

2 Model output and observational data

In this study, the hindcasts from the NCEP CFS version 2 (CFSv2) are analyzed. The CFSv2 is a coupled atmosphere–ocean–land–sea ice dynamical seasonal prediction system. It replaced the CFS version 1 (Saha et al. 2006) in March 2011. The atmospheric component is the NCEP Atmospheric Global Forecast System (Moorthi et al. 2001) with a T126 horizontal resolution and 64 sigma layers in the vertical. The oceanic component is the Geophysical Fluid Dynamics Laboratory Modular Ocean Model version 4 (MOM4; Griffies et al. 2003), and the land model is the NCEP, OSU, Air Force, and Hydrologic Research Laboratory model (Noah; Ek et al. 2003). The different components are coupled without flux adjustment, and the initial conditions are obtained from the Climate Forecast System Reanalysis (CFSR; Saha et al. 2010).

We analyze the output from the retrospective forecast of 45-day integrations by CFSv2 initiated from every 0, 6, 12, 18 UTC cycle from 1999 to 2009, and only the daily output for 500-hPa geopotential height, 850- and 200-hPa winds, surface temperature, and precipitation are analyzed. The observations used for model verification includes atmospheric variables and surface temperature from the CFSR and the Climate Prediction Center Merged Analysis of Precipitation (Xie and Arkin 1997). The CFSR is a coupled atmosphere–ocean–land–sea ice reanalysis product and it provides reliable estimate of the atmospheric and oceanic state (Xue et al. 2010; Wang et al. 2010).

In this study, biases for subseasonal prediction are examined for monthly means and pentad means. While the former only presents an overall background of biases, the latter shows the detailed time evolution of the biases and subseasonal features are thus focused. For a specific predicted target month (or pentad), lead 0 is defined as the model runs initialized on the first day of the month (or pentad), lead 1 denotes the model runs initialized on the last day of the previous month (or pentad), lead 2 for the forecasts initialized second to the last day of the target, and so forth until a maximum of lead 14 for monthly mean and a maximum of lead 40 for pentad mean. To make a full use of the reforecast data, in Sect. 3, the prediction for a certain month is an ensemble mean of 60 members with the leads from zero to 14 days. In Sects. 4–6, the ensemble predictions for a certain pentad are divided into eight groups according to the length of lead time, i.e. 0–4, 5–9, and every 5 days to 35–40 days. Most of these pentad predictions are ensemble means of 20 members within 5-day leads, except that the last prediction is an ensemble average of 24 members within 6-day leads.

3 Predictions of monthly climatological features

Figure 1 presents the climatologies of monthly precipitation and 850-hPa winds for CFSv2 prediction and its differences from observations from April to August. Ensemble means of leads of 0–14 days for target months (see Sect. 2 for specification of initial conditions) are shown for discussion of CFSv2 prediction in this section. The distribution in September is not shown because of its similarity with previous months. The model captures the major evolution features of ASM, which include: the eastward retreat of the western Pacific subtropical high (WPSH); the commencement of the tropical Asian monsoon in May; the development and prevalence of tropical westerly wind and precipitation in June and July; and the decline of monsoon in August. Model results also agree with observations (figure not shown) in the locations and magnitude of major rainfall in many places. However, apparent systematic biases of the model exist, including the southerly wind bias over Somalia, the westerly wind bias over the eastern tropical Indian Ocean (ETIO), the easterly wind biases over Indian Peninsula (IP) and Indo-China Peninsula (ICP), the northerly wind bias over the Southeast Asia (SEA), and the cyclonic wind bias over the NWP.

Consistent with the above wind biases, wet bias is found over ETIO and dry biases appear over the Bay of Bengal (BOB), SEA, and the western edge of WPSH. Also, there are centers of wet bias at the southern edge of the Tibetan Plateau (TP) and the west coasts of IP and ICP, which may be due to the unreasonable estimation of the influence of topography in the model. In addition, the seasonal differences of biases are substantial. For example, easterly wind bias over ETIO in April and May is replaced by oppositely signed bias from June to August, and the shift of position of main bias over NWP is similar to that of WPSH. It should be pointed out that, the significant dry biases over the BOB and the South China Sea, as well as the wet biases over the southern flank of TP and the west coast of ICP, also appeared in the CFS version 1 (Yang et al. 2008a; Drbohlav and Krishnamurthy 2010) and some multi-model ensemble products (Lee et al. 2010; Preethi et al. 2010; Li et al. 2012; Rajeevan et al. 2012), suggesting a deficiency of state-of-the-art climate models. Nevertheless, the biases over the tropical Indian Ocean in CFSv2 show partially different features from other coupled models, which often show wet and dry biases over the western and eastern tropical Indian Ocean, respectively.

Outgoing longwave radiation (OLR) and 200-hPa winds are also examined (figures not shown). As suggested by the OLR, rising motion appears over ETIO and sinking motion over IP, ICP, and SEA, along with high-level northeasterly wind anomalies across these areas. These features imply a bias of Hadley-cell type anomaly imposed on the meridional

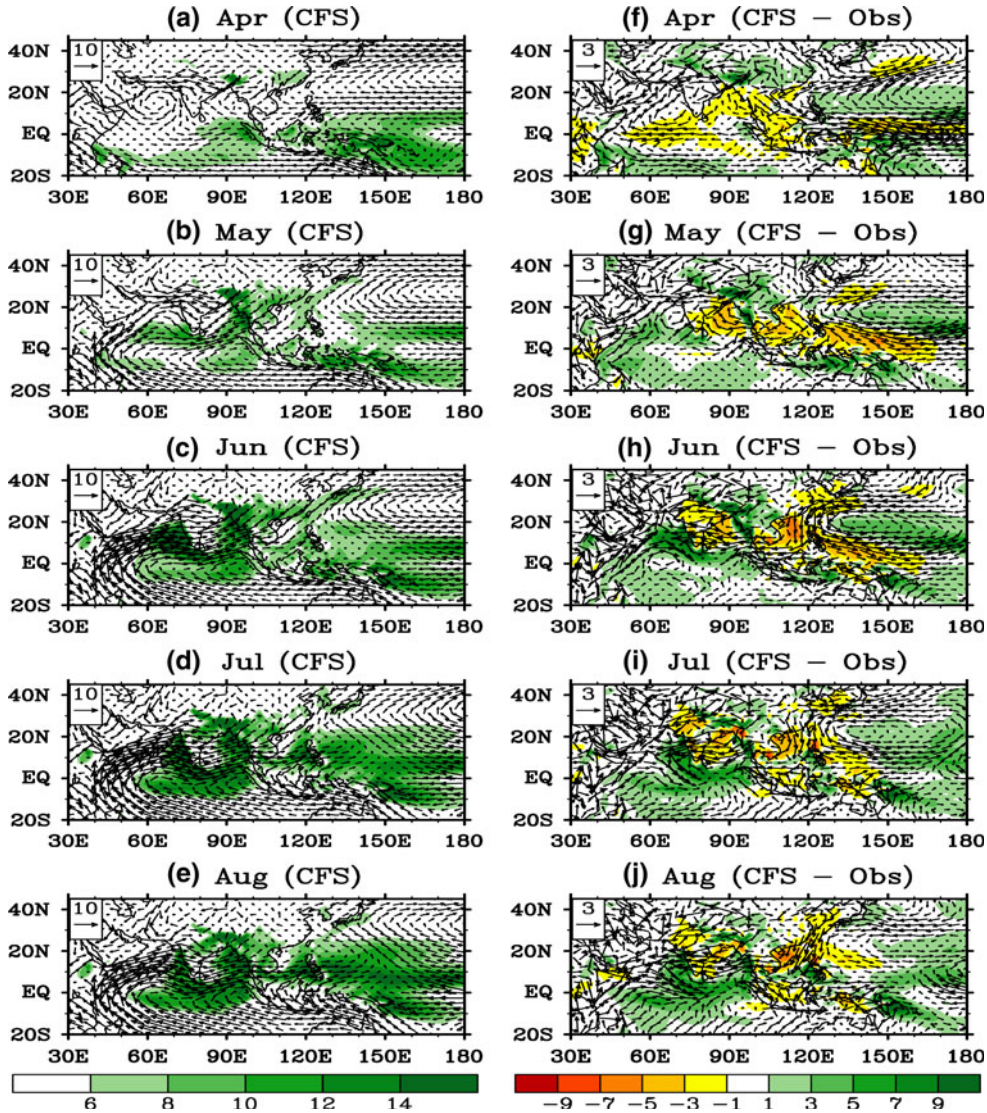

Fig. 1 Monthly precipitation (*shadings*, units mm/day) and 850-hPa winds (*vectors,* units m/s) for CFSv2 (*left column*) and its differences from observations (*right column*) from April to August

monsoon circulation. There is also a bias of anti-Hadley-cell type anomaly over the NWP. The above features indicate that the prediction of the Asian monsoon by CFSv2 is typically characterized by a systematically weaker-than-observed monsoon circulation.

We further plot the time-latitude cross sections of predicted and observed precipitation, as well as their differences, along 70°–90°E, 90°–110°E, and 110°–130°E for the monsoons over IP, ICP, and SEA, respectively. As shown in Fig. 2a–c, the evolution of the tropical monsoon is characterized by a large spatial scale process in which heavy precipitation migrates from the equator in spring to the subtropical Asian land in summer and retreats to the equator in fall and winter. Nevertheless, the onset and decay features of the monsoon exhibit geographical differences. Typically, the ASM shows a gradual northward shift in May and a quick southward withdrawal in September over the IP, a quick northward extension in May and a slow southward retreat in September over SEA, and transitional features (between the above two) over the ICP.

Figure 2d–i show that the CFSv2 reasonably captures the onset and retreat of the tropical monsoons over South and East Asia. However, for the peak monsoon period, the model shows insufficient precipitation over most regions from IP to SEA, except for the longitude band of 90°–110°E near 15°N, where rainfall is overestimated over the west coast of the ICP. In addition, excessive rainfall appears over ETIO and the southern edge of the TP throughout the entire monsoon season.

We plot the differences in surface temperature between CFSv2 and observation in Fig. 3. Clearly, there is a warm bias in the western tropical Pacific and a cold bias in the northern subtropical Pacific, which may be related to the apparent dry bias at the western edge of WPSH and the upwelling of cold water at the northern edge of WPSH due to the impact of a cyclonic wind bias over the NWP.

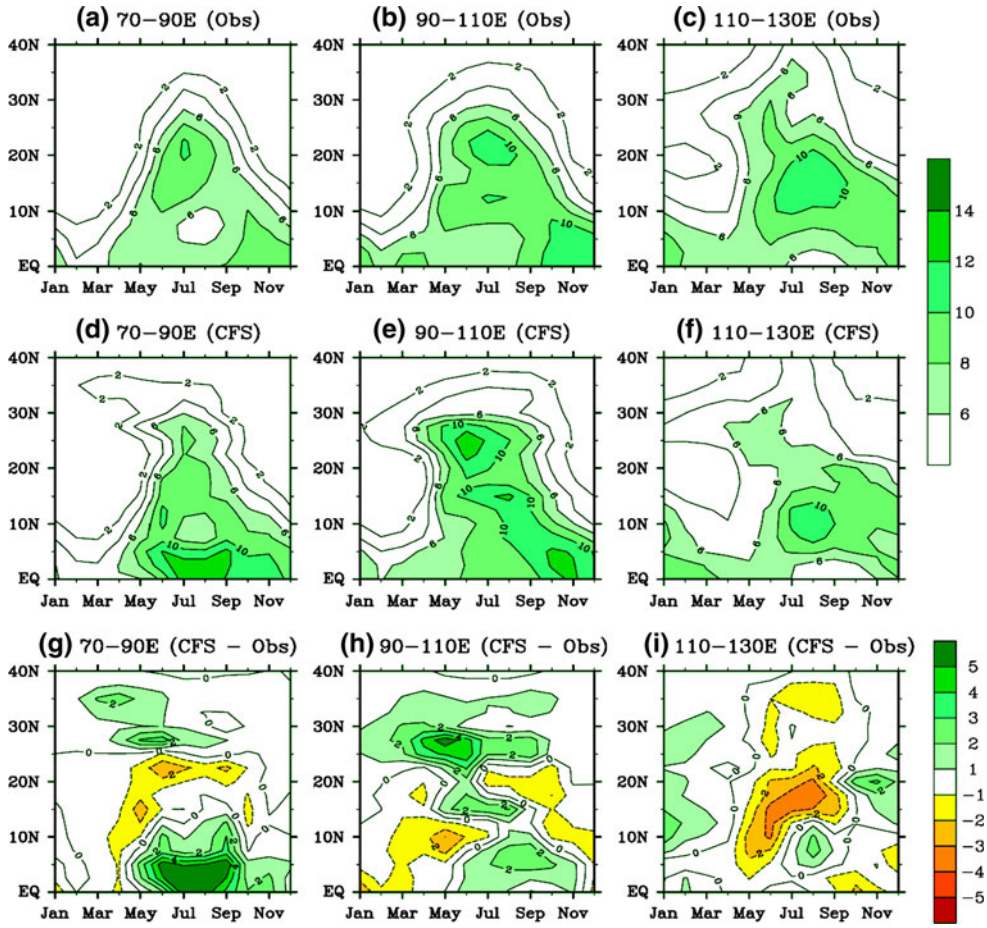

Fig. 2 Latitude-time cross sections of monthly precipitation (units mm/day) along 70°–90°E (*left column*), 90°–110°E (*middle column*), and 110°–130°E (*right column*). **a–c** are for observations, **d–f** for CFSv2, and **g–i** for the differences between model and observations

During the summer monsoon season, most of the subtropical land from North Africa to the western TP experiences significant warm biases, while the subtropical land of East Asia is mainly dominated by a cold bias. However, there seems to be a cooling tendency from May to August for the warm biases over the subtropical land to the north of IP and BOB, where a more apparent transition from positive to negative bias occurs simultaneously in 500-hPa geopotential height (figure not shown). Moreover, the warm biases of surface temperature in ETIO in April and May are replaced by cold biases from June to August.

4 Subseasonal evolutions of tropical winds and rainfall

We now examine the variations of pentad rainfall and winds. Figure 4 shows the biases of pentad mean precipitation and 850-hPa winds in different periods of summer monsoon season for the predicted ensemble average of time leads of 0–4 days. The chosen periods include 1–5 May, 11–15 May, 31 May–4 June, 10–14 June, 30 June–4 July, 10–14 July, 30 July–3 August, and 9–13 August. The pentad predictions with such short leads are thought to be the most skillful forecasts that the model can make, but significant systematic biases are still found. Similar to the features shown in Fig. 1, weaker zonal wind over the tropical monsoon region and cyclonic wind bias over the NWP exist in the different development stages of ASM. Correspondingly, dry biases dominate over the IP, BOB, and SEA. Figure 5 further shows the predictions with time leads of 35–40 days, which may not be skillful, but helpful for revealing the growth of biases with lead time. From the shortest-lead to the longest-lead predictions, the easterly wind bias over South Asia and the cyclonic anomaly bias over NWP strengthen significantly. Meanwhile, in the tropical area near South Asia, as well as over the central area of cyclonic wind bias over NWP, there is a remarkable growth of wet biases consistent with the formation of large convergence biases. Also, the dry bias at the western edge of WPSH may be stronger in predictions with long leads than with short leads before late June, even this feature seems opposite after late June. However, overall, there are a decrease in the dry bias and an increase in the wet bias over the entire Asian monsoon region. Nevertheless, the

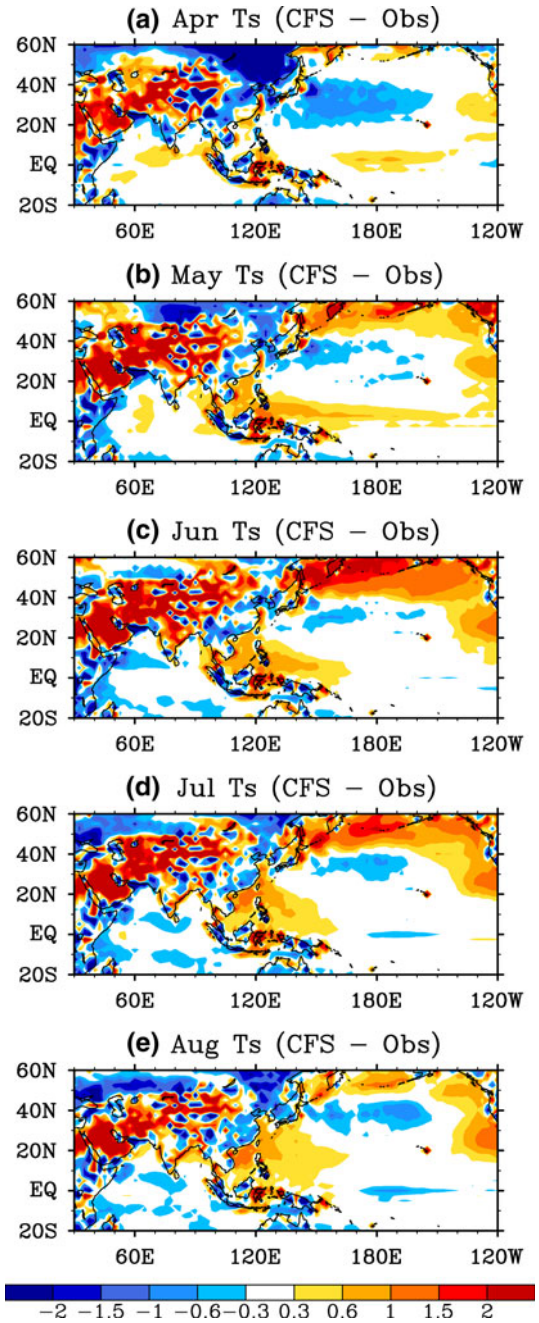

Fig. 3 Differences in monthly surface temperature (units °C) between CFSv2 and observations (model minus observations) from April to August

dry bias over IP and BOB does not show clear growth although the associated zonal wind further weakens from short to long leads.

To depict regional monsoons, we analyze the area-averaged zonal wind and precipitation over the IP (100°–20°N, 70°–90°E), the ICP (10°–20°N, 90°–110°E), and SEA (10°–20°N, 110°–130°E) (Fig. 6). The predictions of all leads have significant correlation with observations due to the consistent prediction of the seasonal trend, with the predictions of short lead time capturing the subseasonal variation of the monsoon reasonably well in spite of systematic biases.

It is generally assumed that variation consistency and amplitude difference, measured by correlation and root mean square error (RMSE) respectively, should have the highest skill at the minimum lead time, followed by a gradual reduction with increasing lead time owing to the decay of initial memory of the coupled system. However, the predictions of regional monsoons do not fully conform to the above notion. First, the RMSE of precipitation over tropical monsoon regions, especially over IP and ICP, is not always the smallest at the minimum lead time, which may be attributed to the high noise related to the initial shock of the forecast system. Secondly, the forecast skill which decreases with increasing lead time can increase again after the lead time longer than 1 month, perhaps because the atmospheric initial memory has lost significantly at that lead and predictions begin to be dominated by slowly varying components of the climate system.

Figures 7, 8 and 9 show the observed and predicted zonal wind and precipitation with different leads along 70°–90°E, 90°–110°E, and 110°–130°E, respectively. The cross section of observed zonal wind along 70°–90°E is characterized by a quick northward shift from the equator to the IP in late May and June and a rapid southward retreat from the IP to the equator in late August, with a maximum wind center over the IP in mid-August (Fig. 7). However, the predictions show differences from observation due to bias growth. The forecasts with leads of 0–4 days show best agreement with observation, but they display weaker zonal wind over the IP and stronger wind over the tropical Indian Ocean, where a maximum center forms around June. With increasing lead time, the predicted zonal wind over the IP often has a clear reduction in intensity and duration. Interestingly, the zonal wind over the tropical Indian Ocean often maintains an equivalent strength with observation at the leads from 0–4 days to 20–24 days, and afterwards an increasingly significant positive bias appears during the entire summer season. Over the IP, the precipitation is heavy at the leads of 0–4 days, and diminishes from 5–9 to 25–29 days, followed by reinforcement again from the leads of 30–34 days. Over the tropical Indian Ocean, the predicted precipitation already has a positive bias at the short lead, which strengthens gradually and peaks at the leads of 25–29 days.

Figure 8 displays that the zonal wind over ICP is underestimated at the short lead and its intensity shows an apparent reduction with the increase of lead time until reaching leads up to 25–29 days when the zonal wind intensifies again with its center slightly shifted southward to the tropical Indian Ocean. The precipitation field is also featured by the overestimated rainfall over the tropical

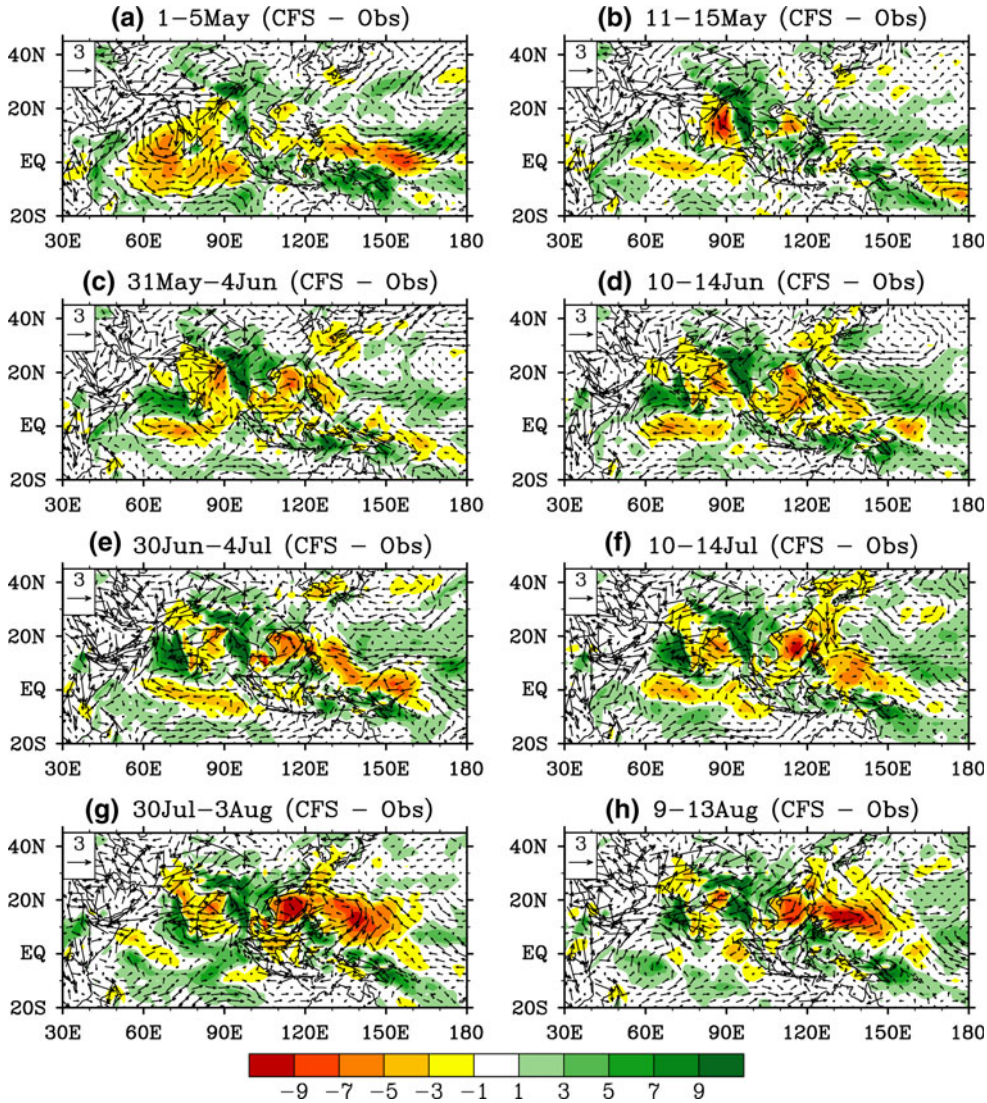

Fig. 4 Differences between predictions and observations for pentad precipitation (*shadings*, units mm/day) and 850-hPa winds (*vectors,* units m/s) in different periods of summer monsoon season for predicted ensemble averages with lead time from 0 to 4 days

Indian Ocean in the long-lead forecasts, and in most cases the position of the rain belt over the ICP is farther north than observed, resulting in a dry bias in the southern portion of the ICP and a wet bias in the north. In addition, the large wet bias to the southern edge of TP, associated with the corresponding westerly anomaly bias, exists in the entire monsoon season.

Figure 9 indicates that the zonal wind over SEA does not show a gradually intensifying systematic bias in most predictions, although it is also clearly overestimated in the equatorial areas and southern SEA in the forecasts with leads longer than 25–29 days. However, there is a persistent large dry bias over SEA, and the rainfall is mainly limited to the southern regions, which is especially noticeable in the long-lead predictions. It seems that over SEA the zonal wind bias does not match the precipitation bias, as previously shown in Figs. 4 and 5. The reason for this feature is likely attributable to the dry bias related to the northerly wind bias over SEA, which is always part of the cyclonic wind bias over the NWP. It should also be noted that the zonal wind and precipitation over SEA in late May and East China in late July are also underestimated in most predictions.

Overall, the development of biases shows disparity between winds and precipitation, as well as spatial difference between tropical monsoon regions and equatorial areas. However, a prominent feature is that systematically weaker zonal wind and highly-varied precipitation tend to appear over the IP and the ICP for most predictions while stronger winds and heavier rainfall occur over the ETIO for the long-lead predictions. Also, along with the strong dry bias over SEA in all forecasts during most of the monsoon season, the overestimated rainfall over southern SEA and its adjacent equatorial region tends to be increasingly significant with the advance of lead time.

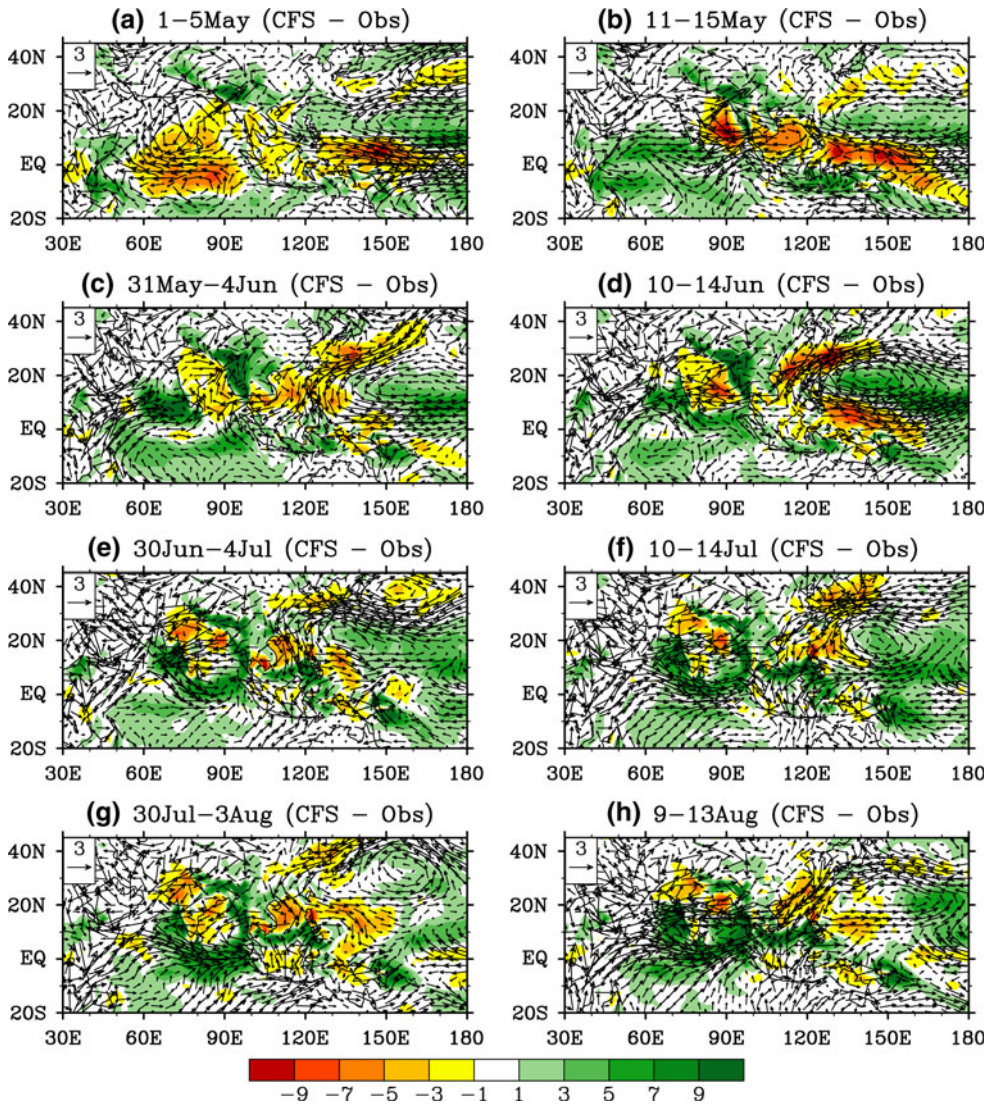

Fig. 5 Same as Fig. 4 but for the ensemble predictions with lead time from 35 to 40 days

5 Subseasonal variations of spreads and errors

We use 2 weeks as a cut-off point to distinguish short-lead forecasts and long-lead forecasts and further investigate bias development in the CFSv2. Figure 10 gives the spread of pentad predictions with leads of 0–14 and 15–40 days for 850-hPa zonal wind for different time periods. The spread, also considered as "noise", is defined here as the standard deviation of ensemble members with different lead time, from which we can examine the dispersion of ensemble predictions. We can also understand when and where the noise develops significantly and leads to rapid error growth.

A comparison between short-lead and long lead predictions (Fig. 10a, b) shows important features regarding the noise development of zonal wind. First, the noise growth of zonal wind over the NWP is mainly concentrated in the predictions with lead time less than 2 weeks. Secondly, for a majority of the short-lead predictions the spread of the zonal wind over southern Asia is not as prominent as that over the NWP. However, from July the former intensifies while the latter begins to intensify at a slower pace than before. For predictions with leads of 15–40 days, there is almost no significant spread over southern Asia and the Indian Ocean before late June, when the forecasts with different leads embark on a gradual increase in spread over the ETIO and the equatorial region to the south of SEA. The most significant spread appears in late July.

Figure 11 further shows the spread of pentad predictions with leads of 0–14 and 15–40 days for precipitation in different periods. For short-lead forecasts (Fig. 11a), large spread is mainly distributed over southern Asia, the tropical Indian Ocean, and the western Pacific. The spread over the NWP, mostly characterized by a concentrated distribution along the edge of the WPSH, should be related to the

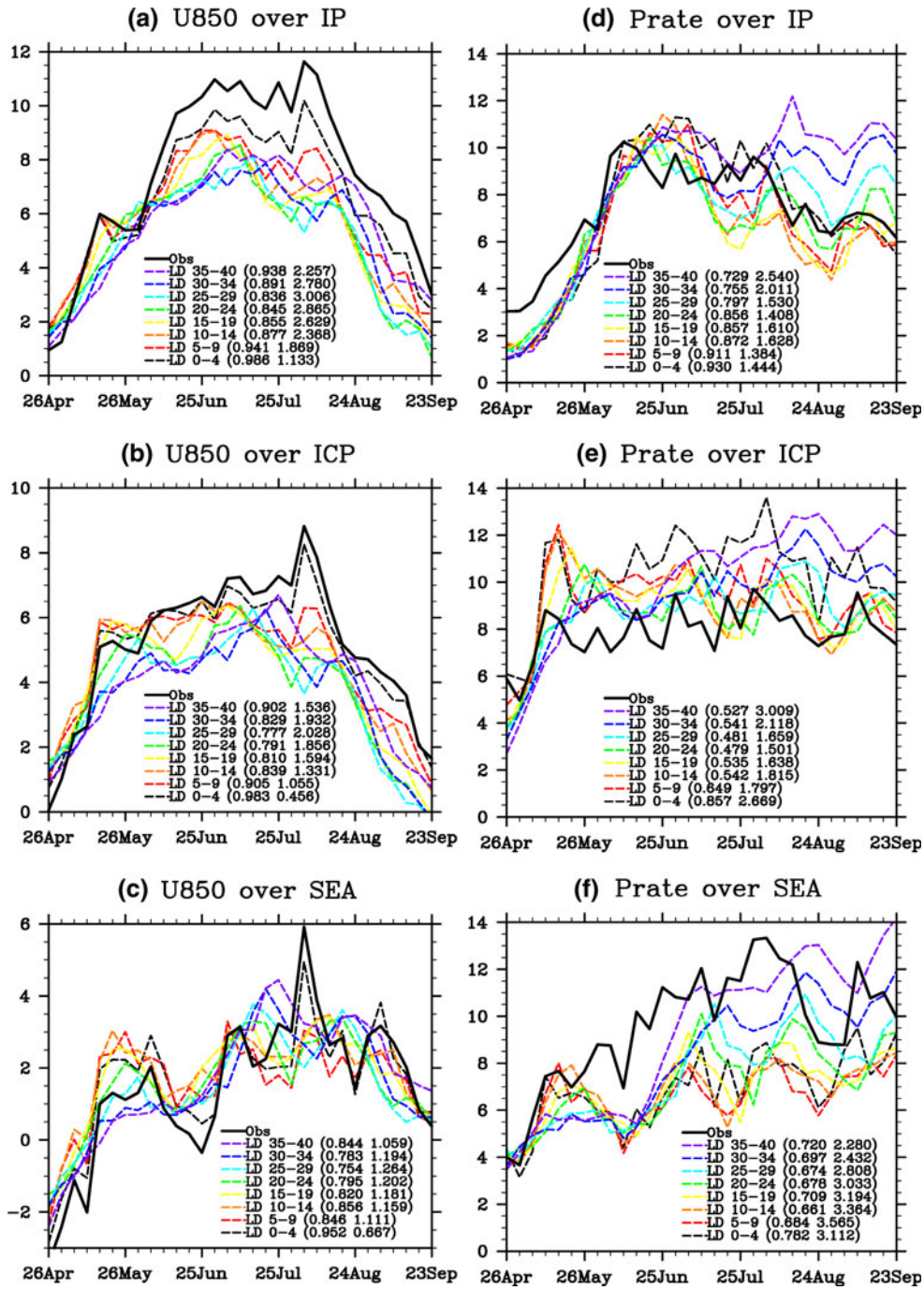

Fig. 6 Variations of pentad 850-hPa zonal wind (*left column*, units m/s) and precipitation (*right column*, units mm/day) averaged over the Indian peninsula (10°–20°N, 70°–90°E), the ICP (10°–20°N, 90°–110°E), and the SEA (10°–20°N, 110°–130°E) for observations and CFSv2 ensemble averaged predictions with different leads of time. The values in each bracket in the legends are temporal correlation and RMSE between predictions and observations respectively

cyclonic wind bias during predictions. Similar to the zonal wind over southern Asia, the spread of precipitation over ETIO also becomes significant from July, which corresponds to the intensification of wet bias over ETIO in predictions with lead time up to 2 weeks, as already shown in Fig. 7b. Since middle and late May, there is a consistent development of spread on the west coasts of IP and ICP for short-lead predictions. For long-lead forecasts (Fig. 11b), the magnitude of spread over the BOB, the ETIO, the equatorial region to the south of SEA shows more distinct differences between the periods before and after late June. This feature may be partially related to the intensifying wet biases over these regions with increasing lead time for long-lead predictions, as revealed by Figs. 7, 8 and 9. The comparison between Fig. 11a, b further indicates that the predictions of precipitation over the NWP before late June shows a reduction in spread from short leads to long leads. However, after late June, there is still significant spread over the western equatorial Pacific for long-lead predictions, in spite of the small spread near the northwestern edge of WPSH.

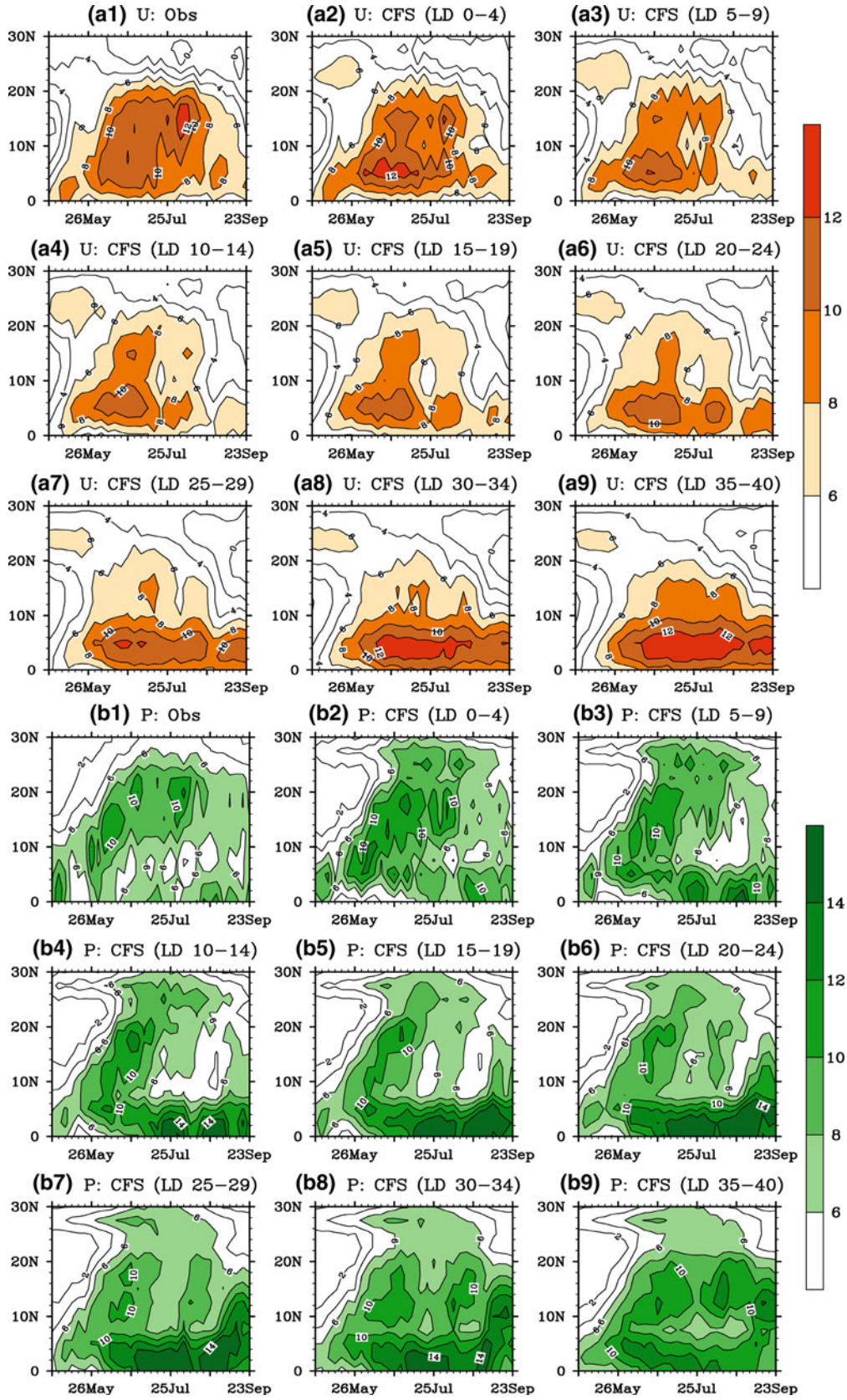

Fig. 7 Latitude-time cross sections of 850-hPa zonal wind (*top three rows*, units m/s) and precipitation (*bottom three rows*, units mm/day) along 70°–90°E for observations and ensemble averaged predictions with different leads of time

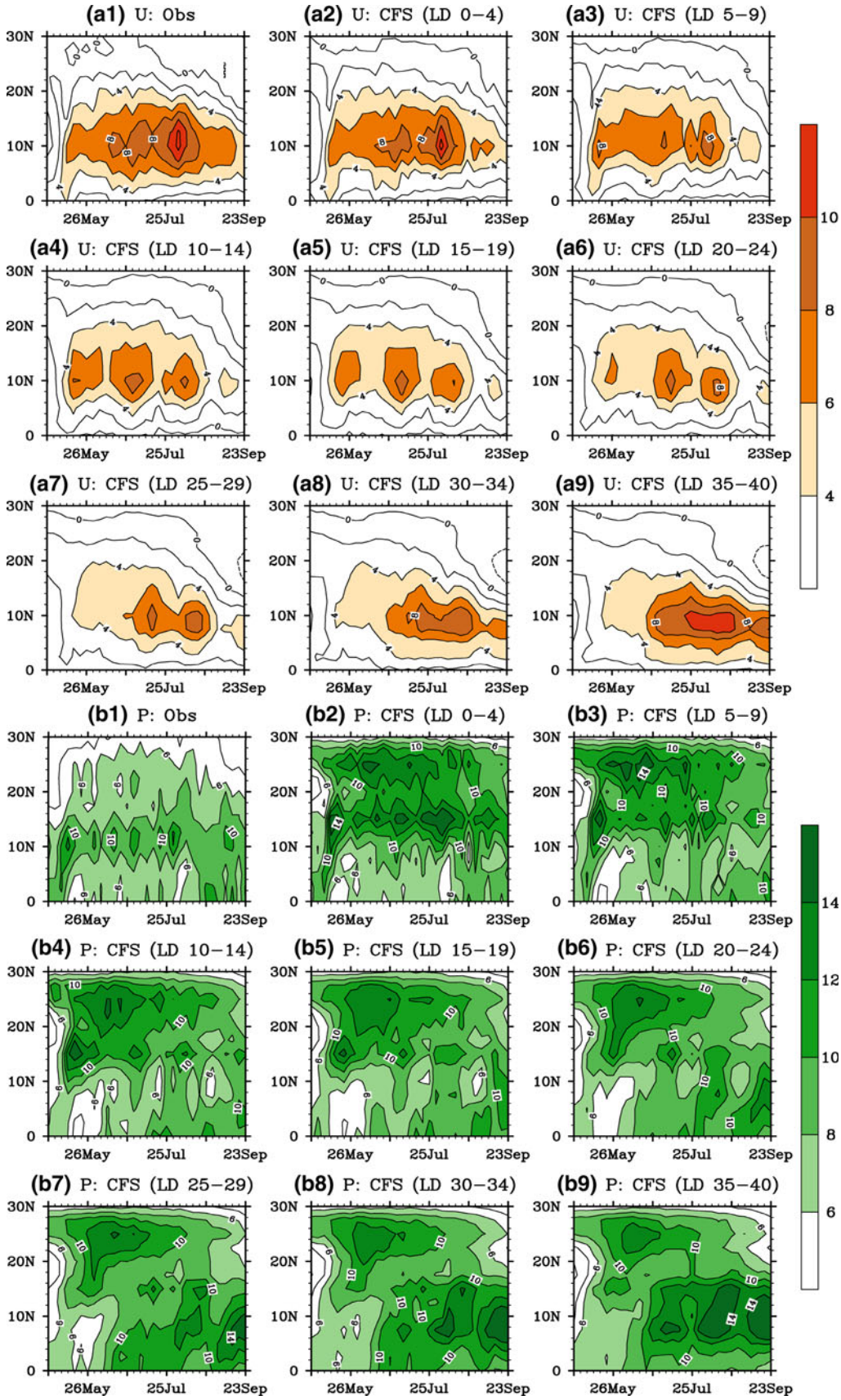

Fig. 8 Same as Fig. 7 but for the latitude-time cross sections along 90°–110°E

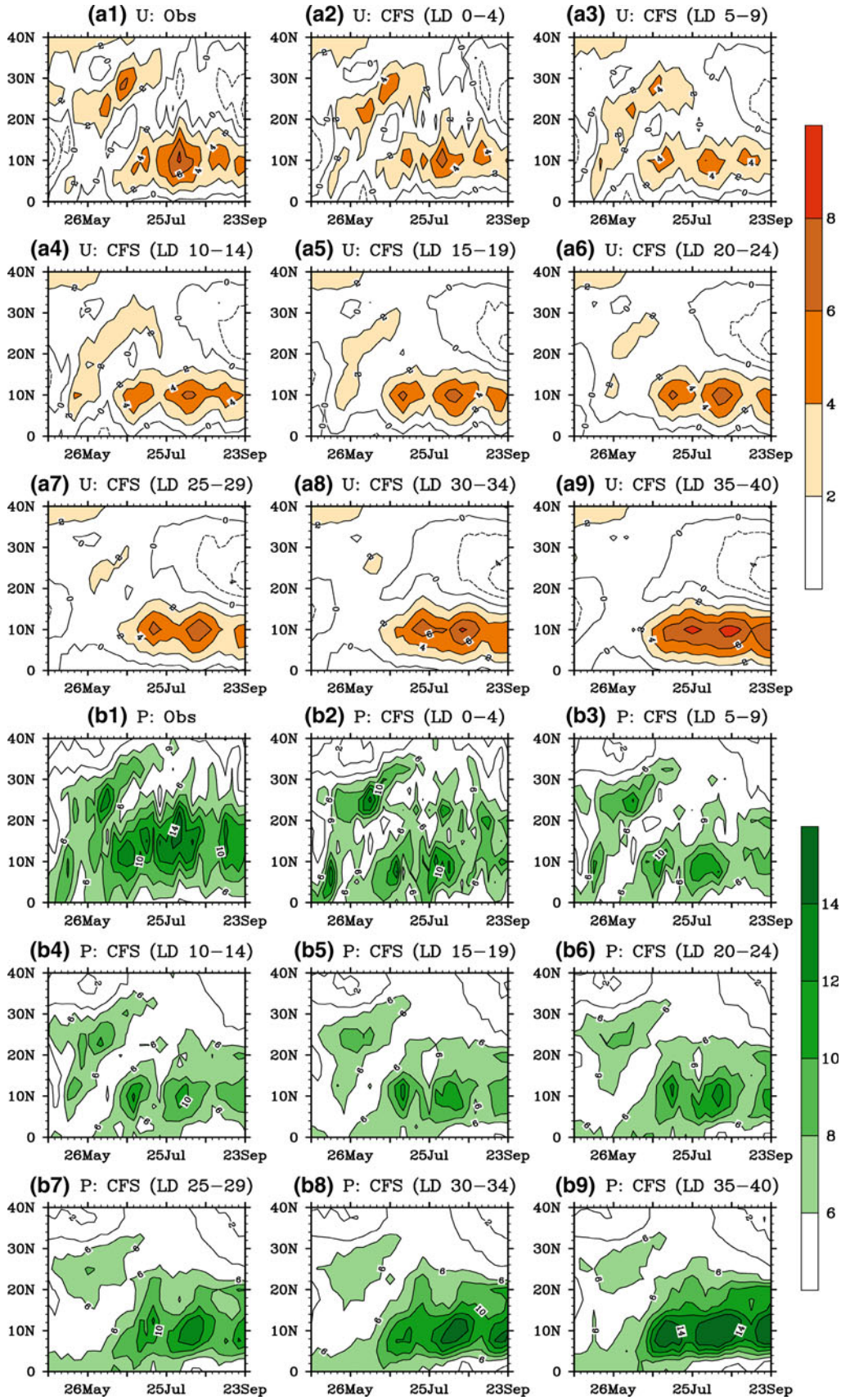

Fig. 9 Same as Fig. 7 but for the latitude-time cross sections along 110°–130°E

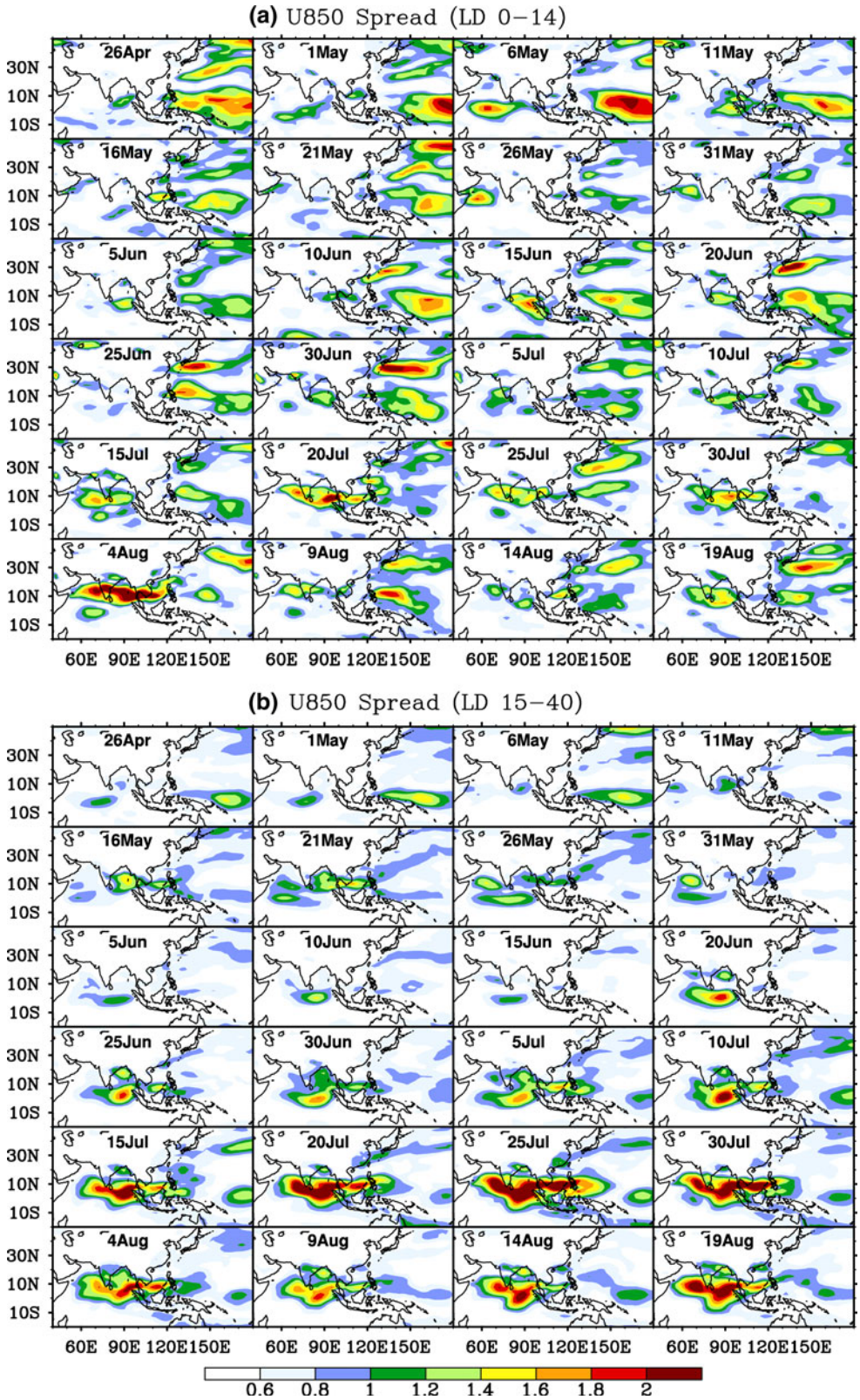

Fig. 10 Spread of pentad predictions with lead time from **a** zero to 14 days and **b** 15–40 days for 850-hPa zonal wind (units m/s) in different time periods. The marked date in each map denotes the pentad beginning with that day

We further analyze the variations of pentad RMSE of 850-hPa zonal wind and precipitation over southern Asia (10°–20°N, 70°–110°E), ETIO (0°–10°N, 70°–110°E), and NWP (10°S–30°N, 130°–180°E) to investigate the development of errors for the ensemble-mean predictions with different leads. Figure 12 shows that the RMSE variations

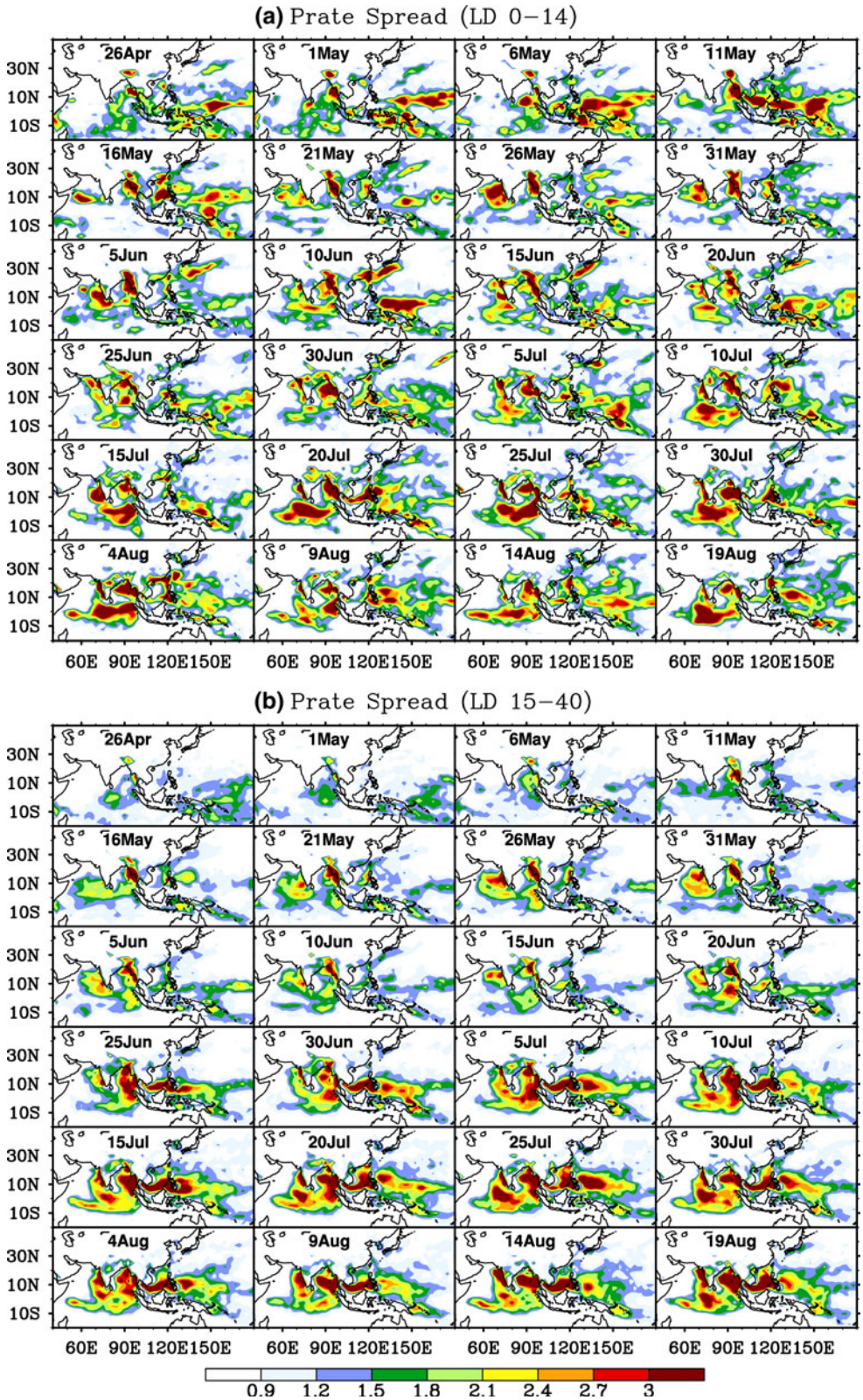

Fig. 11 Same as Fig. 10 but for precipitation (units mm/day)

of zonal wind over southern Asia and ETIO for predictions with different leads are characterized by small (large) dispersion before (after) July. As seen from Fig. 11, this feature means gradual error growth with increasing lead time for the former and diversified distribution of error for the latter. The intensity of precipitation error over southern

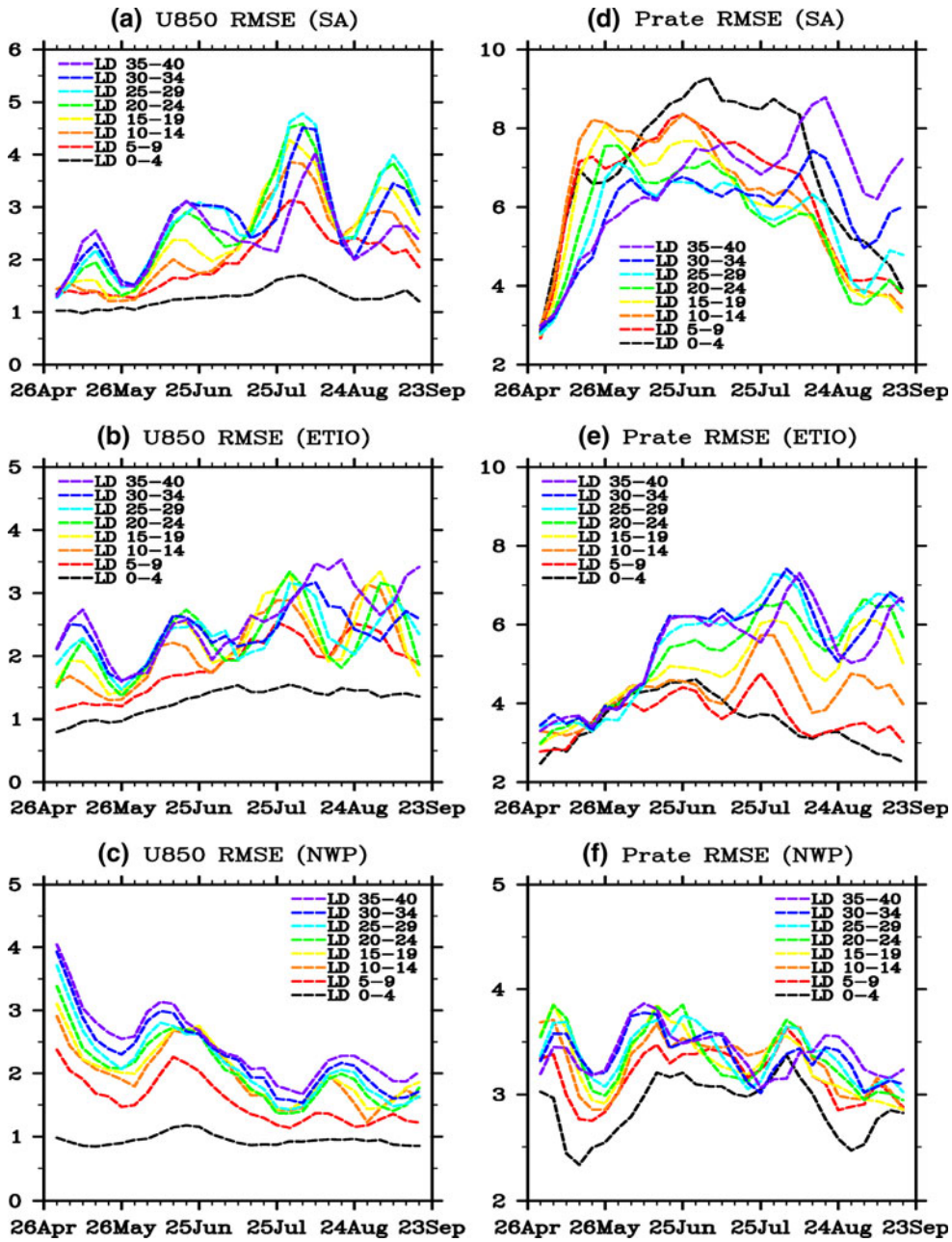

Fig. 12 Variations of pentad root mean square errors of 850-hPa zonal wind (*left column*, units m/s) and precipitation (*right column*, units mm/day) over southern Asia (10°–20°N, 70°–110°E), ETIO (0°–10°N, 70°–110°E), and NWP (10°S–30°N, 130°–180°E) for ensemble averaged predictions with different leads. The *curves* shown are all results postprocessed by 3-point running average

Asia (Fig. 12d) exhibits a seasonal tendency to grow from May to July and a decreasing tendency since mid-August. In addition, predictions of the precipitation over southern Asia show temporal difference in the monsoon season. That is, the dispersion of both short- and long-lead forecasts is not significant before July, when the predictions with different leads begin to show apparent divergence. An especially notable dispersion appears after mid-August. There are no significant differences in the precipitation over ETIO for all predictions before late June (Fig. 12e), after which the short-lead predictions begin to display smaller error but larger dispersion while the long-lead forecasts show opposite features.

Figure 12 further shows that the error growth of zonal wind over the NWP (Fig. 12c) is almost concentrated at the lead time up to 2 weeks and shows little change in long leads. It should be noted that error of zonal wind over the NWP is always larger during long leads than short leads among the whole period of monsoon evolution, and it is significantly larger before late June than after late June in almost all predictions except for the forecast with lead time of 0–4 days. Also, the predicted precipitation over the NWP (Fig. 12f) always shows more rapid and more significant error growth during short leads than long leads before late June. After June, the predictions begin to present apparent dispersion and the errors of short-lead

forecasts are not always smaller than those of long-lead forecasts.

6 Possible causes of biases

The above analysis has clearly shown that the subseasonal prediction of the tropical Asian monsoon largely depends on both lead time and the evolution stage of monsoon. On the one hand, the spread of zonal wind over the NWP shows larger magnitude in short-lead forecasts than in long-lead forecasts, while the predictions of zonal wind over southern Asia and ETIO often exhibit more remarkable spread from July for long leads than for short leads. On the other hand, the error development of zonal wind and rainfall over the above regions, especially southern Asia and the ETIO, sometimes shows marked dissimilarity between the state before late June or early July and afterwards. It seems that a typical split time of major change appears around July, when error growth shows a significant change in the tropical monsoon region and adjacent equatorial areas. Therefore, two questions that need to be answered are what happened and what may be responsible for the features.

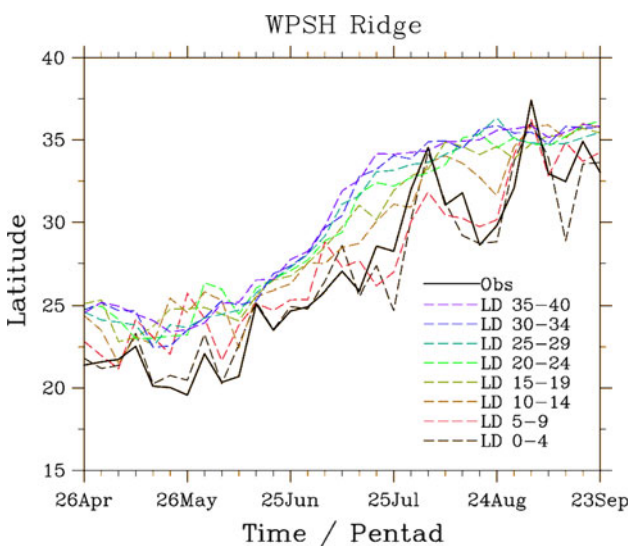

Fig. 13 Variations of the ridge of WPSH for observations and ensemble averaged predictions with different leads

As suggested in Sects. 3 and 4, cyclonic wind bias and its associated precipitation bias are the dominant biases over the NWP, which may be closely associated with the WPSH. Thus Fig. 13 shows the variations of the ridge of WPSH for ensemble-mean predictions with different leads. The ridge is defined as the average latitude of the zero contour of 850-hPa zonal wind within the region of 10°–45°N/120°–150°E. The predictions with leads of 0–4 and 5–9 days capture the observed features of subseasonal variations of WPSH. That is, the ridge maintains its positions near 20°N from late April to mid-June, and then shifts northward to 25°N and maintains that position until mid-July. From middle and late July to mid-September, the WPSH shows two rapid northward jumps followed by an apparent southward retreat, with the northernmost ridge position located near the Korean Peninsula and the Sea of Japan. As lead time increases, the ridge shows an early and slowly northward jump. Around July, the ridge of WPSH is in a northward shifting process in most predictions.

Over southern Asia, the variation of wind and precipitation biases is connected to the evolution of South Asian summer monsoon (SASM). For ensemble-mean predictions with different leads, Fig. 14 shows the variations of two monsoon indices: the Webster–Yang index (WY; Webster and Yang 1992) and the monsoon Hadley index (MH; Goswami et al. 1999). The WY index is defined as the vertical shear of zonal winds between 850 and 200-hPa levels averaged over region 0°–20°N/40°–110°E, and the MH index is defined as the vertical shear of meridional winds between 850 and 200-hPa averaged over 10°–30°N/70°–110°E. The predicted WY index shows a systematic weak bias during the entire monsoon

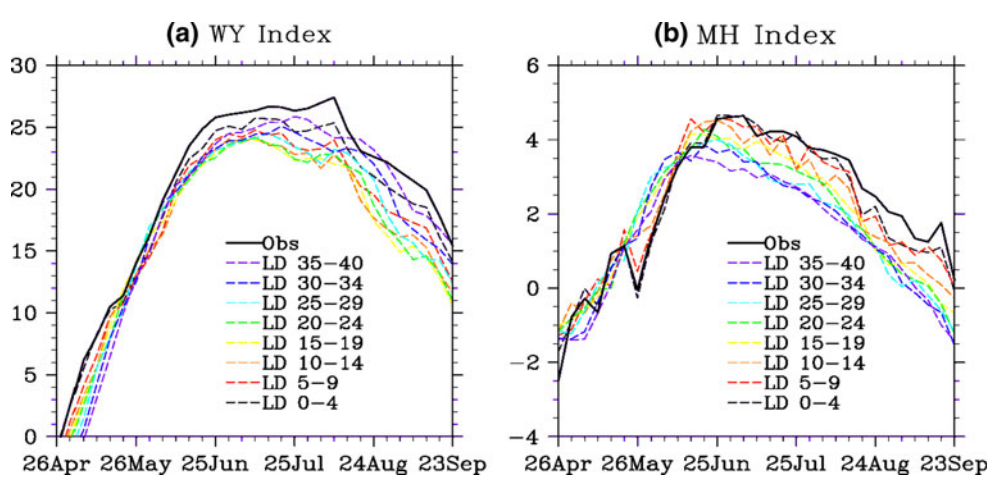

Fig. 14 Variation of the **a** Webster–Yang index and **b** monsoon Hadley index (units m/s) for observations and ensemble averaged predictions with different leads

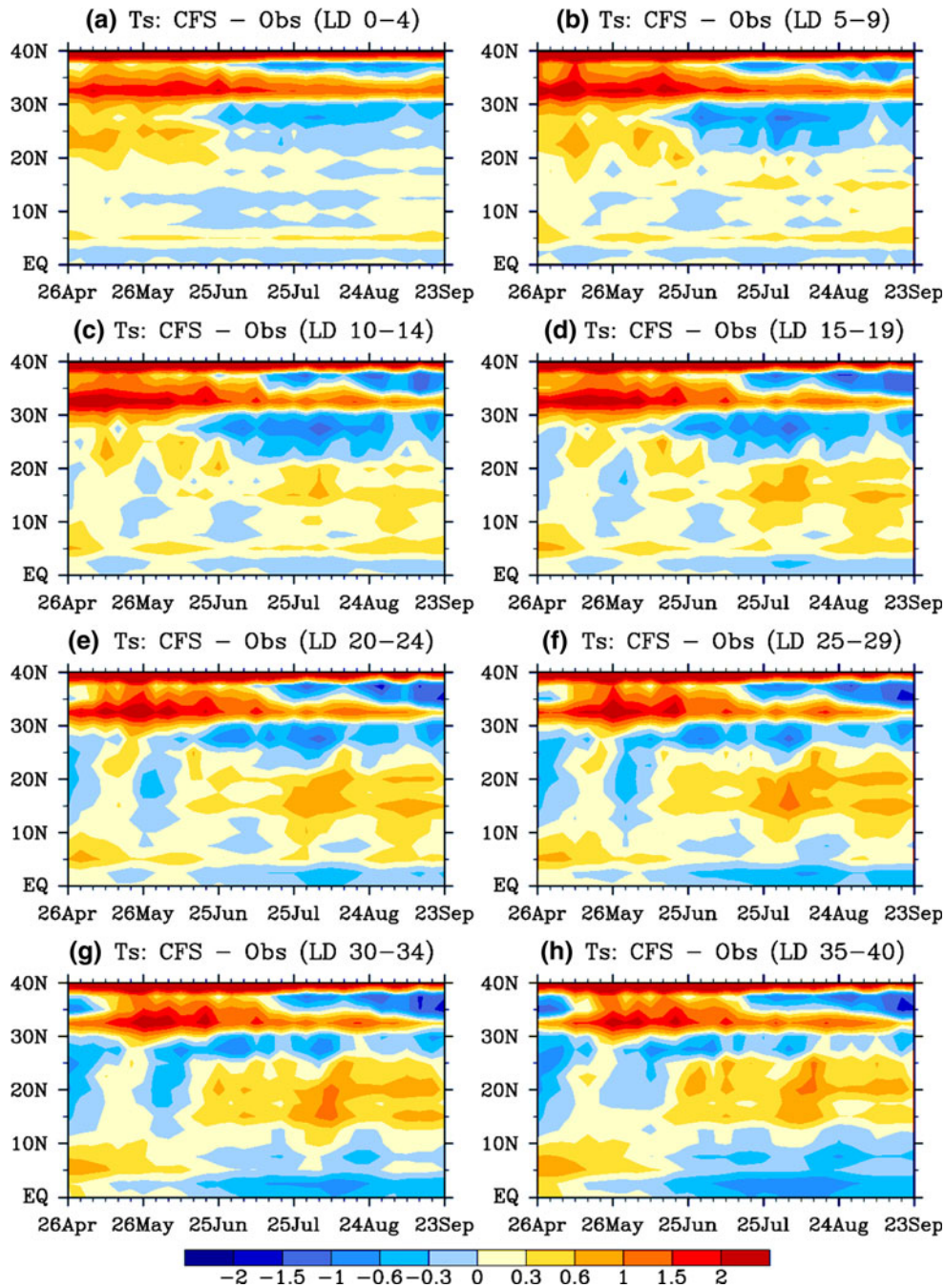

Fig. 15 Latitude-time cross sections of prediction biases of surface temperature (units °C) along 70°–100°E for ensemble averaged predictions with different leads

season, and the bias is especially significant around July. The predicted MH index is also weaker than observed since July, but not before late June. The WY index shows relatively large consistency and a long period of peak time among the various predictions. However, the MH index shows an evident weakening from short leads to long leads after late June, with a short period of peak time. This feature denotes that the SASM peaks around the so-called split time and then withdraws gradually. It is also indicated by Fig. 14b that the longer the prediction leads, the earlier the monsoon reaches the peak and begins a retreat.

Not only the internal atmospheric variability but also external forcing may contribute to the biases and their growth. As depicted by Fig. 3, there is a transition of thermal bias over the subtropical land to the north of IP and BOB during the monsoon season. Does it have a relationship with the features of bias development shown above? We next analyze the latitude-time cross sections of prediction biases of surface temperature along 70°–100°E (including IP and BOB) for ensemble-mean predictions with different leads (Fig. 15). The development of thermal bias shows apparent spatial and temporal differences. First, over the TP (30°–

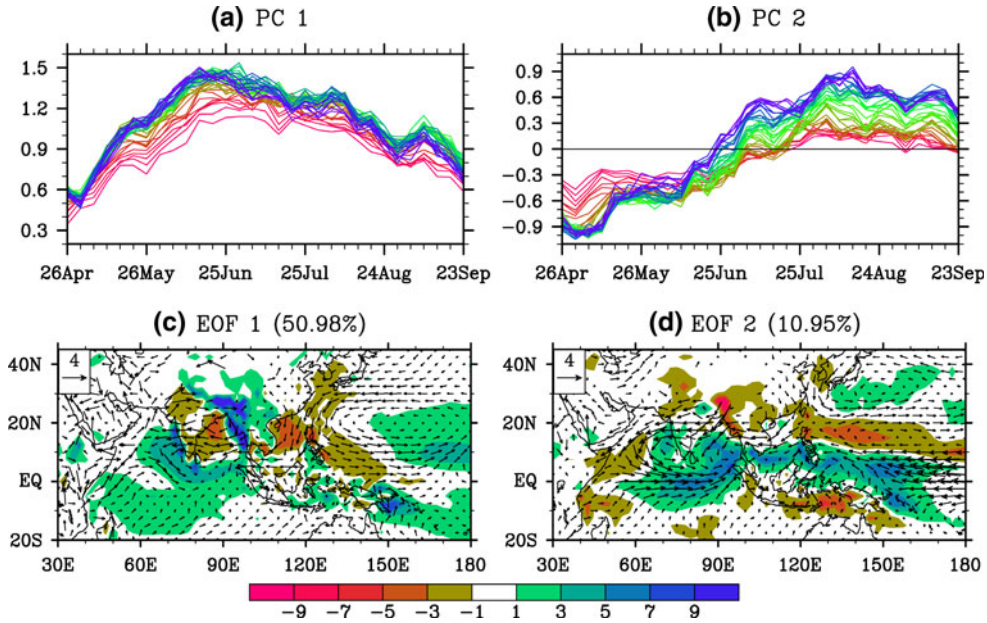

Fig. 16 The first two principal components (*top row*) and leading modes (*bottom row*) of multivariate EOF analysis of the prediction biases of 850-hPa winds and precipitation of all leads. The color range from the *red end* to the *blue end* in **a** and **b** denotes the leads from 0 to 40 days

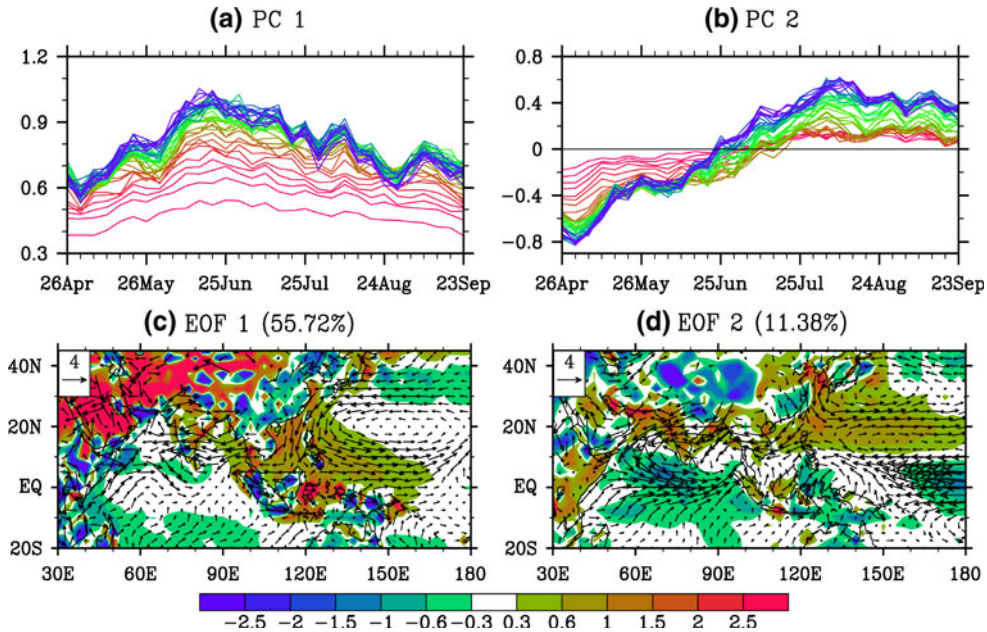

Fig. 17 Same as Fig. 16 but for multivariate EOF analysis of the biases of 850-hPa winds and surface temperature

40°N), the significant warm bias appears in May and June. It weakens gradually from July and is even partially (near 35°N) replaced by a cold bias after mid-July. This difference before and after July is more remarkable in long-lead forecasts (Fig. 15d–h) than in short-lead forecasts (Fig. 15a–c). Secondly, among the latitude belt of 10°–30°N, the surface temperature over subtropical land to the north of IP and BOB shows a transition from warm to cold bias around July in short-lead forecasts. In long-lead predictions the warm bias before July is mostly replaced by a cold bias, along with another transition from cold to warm bias over IP and BOB around July. It can also be seen that, from July, the meridional thermal difference between subtropical land and the tropical IP and BOB is weaker than the observed due to the cold bias over the subtropical land. It further weakens from short-lead to long-lead predictions because of the warm bias over IP and BOB. This feature may be associated with the apparent decline of SASM from short leads to long leads after late June as shown in Fig. 14b. Thirdly, the surface temperature bias in ETIO, which is opposite to the bias over IP and BOB, changes from positive to negative around July in long-lead predictions.

Overall, the WPSH, the SASM, and the thermal state of underlying surface in Indian Ocean and southern Asia show significant changes around the split time of bias development in the subseasonal prediction of ASM. To connect all

these known factors, and gain a more comprehensive understanding of the causes of the biases, a multivariate empirical orthogonal function (EOF) analysis is carried out for the prediction biases of 850-hPa winds and precipitation (Fig. 16), and for the prediction biases of 850-hPa winds and surface temperature (Fig. 17). The predictions of all leads from zero to 40 days are involved in the computation.

The first mode (Fig. 16c) is characterized by an apparent cyclonic wind bias over the NWP and an easterly wind bias over IP and BOB, as well as an anticyclonic wind bias over the western tropical Indian Ocean. Correspondingly, dry biases appear over the BOB, IP, SEA, and the west coast of NWP and a wet bias emerges from the ETIO. In agreement with what has been discussed in Sects. 3 and 4, these biases indicate weaker WPSH and SASM. Meanwhile, along with the similar distribution of wind biases revealed by Fig. 16c, the first EOF mode of winds and surface temperature (Fig. 17c) shows apparent warm biases over SEA and the west coast of NWP, which may be a response to the cyclonic wind bias over the NWP. Apparent features also include the overestimated rainfall over the west coasts of IP and ICP, the warm bias from North Africa to the western TP, and the cold bias over eastern Asia. It should be noted that both modes in Figs. 16c and 17c are highly significant, with a variance larger than 50 percent.

The principal components (PCs), given by Figs. 16a and 17a, show a consistent variation for predictions of all leads: a gradually increasing tendency from May to late June or early July and a slow descent from July to September. Compared to the PCs of short leads, the PCs of long leads show larger values and earlier peaks. The former indicates a decay of initial memory and a growth of prediction bias, while the latter indicates an earlier northward jump of the WPSH and an earlier decline of the SASM as shown by Figs. 13 and 14b. Therefore, the first mode should feature a weak WPSH over the NWP and a weak monsoon over southern Asia. The biases associated with this mode gradually intensify before formation of the strongest SASM and full control of the WPSH over NWP and weaken with the retreat of SASM and WPSH.

The second PC and spatial mode of EOF analysis of winds and precipitation (Fig. 16b, d), as well as of winds and surface temperature (Fig. 17b, d), are further investigated. The bias distribution clearly shows a transition from a negative phase to a positive phase around July, which occurs earlier in long-lead predictions than in short-lead predictions. The transition also corresponds to the split time when the WPSH, the SASM, and the thermal state over southern Asia all show significant changes as shown in Figs. 13, 14 and 15. Associated with the positive phase beginning around July, the second mode is characterized by a development of cyclonic wind bias across IP and ETIO. Accordingly, precipitation is overestimated and may be related to the cyclonic convergence over ETIO (Fig. 16d). Meanwhile, the warm biases over the BOB, the IP, and the Arabian Sea and the cold bias in the ETIO may be associated with weakened westerly wind over southern Asia and strengthened easterly wind over the equatorial region (Fig. 17d). While over the NWP, a wet-dry-wet bias distribution from the equator to the subtropics and an apparent warm bias over most of the subtropical NWP arise as a response to the southeasterly wind bias to the south of 10°N and cyclonic bias to the north of 20°N over the NWP.

The second mode accounts for a smaller variance of about 11 percent; however, its typical features can be captured by the predictions of individual fields because the second mode is in a strong state when the first mode is in a weak state. For example, the negative phase of spatial mode shown in Fig. 16d is similar with the bias distribution depicted in Figs. 1f and 5a, and the positive phase bears much resemblance to the biases over the Indian Ocean and southern Asia as shown in Figs. 1j and 5h. Also, the opposite distribution of biases of surface temperature between the IP and ETIO can be found in the predictions as shown in Figs. 3a, e, and 15e–h. Therefore, the second mode may be related to the transitions of atmospheric circulation and thermal state of the underlying surface. On the one hand, the weak WPSH with a southward position before July can contribute to the cyclonic wind bias to the south of 20°N and the northwesterly wind bias near the equatorial region. The northward shift of the WPSH favors a northward movement of cyclonic wind bias that intensifies the southeasterly wind bias near the Philippines and over equatorial regions. Associated with the evolution of wind bias, precipitation and surface temperature biases over the NWP are replaced by opposite-sign biases during the transition process. On the other hand, the transition from an anticyclonic bias to a cyclonic bias over the Indian Ocean should be closely connected with the regional surface temperature biases and partly attributed to the significant change in surface temperature from warm bias to cold bias over the TP (shown in Figs. 3, 15, 17b, 17d). These features are favorable for a change in the zonal wind to the south of TP from easterly to westerly wind bias as a thermal response of regional atmospheric circulation.

Moreover, as pointed out above, biases do not always increase with increasing lead time. Knowing the time for biases to reach a saturation state may be helpful for identifying their possible source. As shown in Sect. 5, bias development depends on both lead time and the evolution stage of the monsoon. Figures 16 and 17 further verify that the bias growth shown by the first mode is mainly concentrated within the leads less than 2 weeks, which possibly means that the weak WPSH and SASM are primarily internally produced in the atmosphere (when biases in

predicted SSTs are small). Conversely, the biases in the positive phase of the second mode show a gradual increase only when time lead is longer than 2 weeks and hence they may partially result from a response to the biases of slow-varying components.

7 Summary and discussion

In this study, we have diagnosed the biases of subseasonal predictions of the Asian summer monsoon using retrospective forecasts by the NCEP CFSv2. Since the predictions are issued every day with an integration time of 45 days, we are able to understand the biases of subseasonal variations of winds and precipitation, investigate the dependence of biases on prediction period and lead time, and explore the possible physical causes.

Most of the predictions are characterized by conspicuous biases which are obviously dependent on the stages of monsoon evolution and lead time. The biases that have the longest duration and the most apparent development during monsoon season are the cyclonic wind bias over the NWP, the easterly wind bias from the IP to the ICP, the dry biases over the IP, the BOB, and the west edge of WPSH, and the wet bias over the ETIO. These features imply that a weaker ASM is often predicted by the model. However, these biases do not always clearly appear during the entire summer or in the predictions of all lead times. In fact, the biases of winds and precipitation over southern Asia and ETIO are sometimes opposite to each other during different evolution stages of the tropical monsoon. The biases of precipitation are dependent on lead time and they do not always show smaller magnitude in the short-lead predictions when compared to the long-lead predictions.

A further analysis of the spread and RMSE of ensemble predictions indicates that the development of zonal wind and precipitation biases in the ASM region evidently depends on prediction period and lead time. There is a typical split time in late June or early July, when bias development shows a significant change in the Asian monsoon region and its adjacent areas near the equator. In addition, the biases associated with weaker WPSH, especially the zonal wind bias over NWP, always show concentrated development in short-lead (shorter than 2 weeks) predictions, while the biases over southern Asia and ETIO exhibit complicated variations and show more remarkable spreads during long leads (longer than 2 weeks) than short leads after late June.

Bias fields of different variables on all leads are linked by the use of multivariate EOF analysis to explore the possible physical causes of biases. The first mode is featured by a weaker SASM and WPSH compared to observations, and the biases represented by this mode show first an increasing tendency and then a decreasing tendency with the transformation time appearing around late June and early July. The second mode indicates a transition from anticyclonic to cyclonic wind bias in the SASM region, and from the northwesterly wind bias in the equatorial region and anticyclonic wind bias in the subtropics to a southeasterly wind bias and cyclonic wind bias over the NWP. The fundamental change depicted in the second mode also occurs around the same split time mentioned above.

The precipitation and surface temperature biases are consistent with wind biases, and their significant changes around July are likely related to the northward shift of the WPSH and the reversal of surface thermal biases over the TP, southern Asia, and the ETIO during SASM withdrawal. Furthermore, it is suggested that the underestimated WPSH and SASM are mainly internally produced in the atmosphere since bias development in the first mode is often limited to the leads less than 2 weeks. Conversely, from July, the biases in the second mode show a gradual increase only in the lead time longer than 2 weeks, denoting that the biases, likely from slowly varying components such as land and ocean, may partially contribute to the intensification of wind and precipitation biases.

This study focuses on the systematic biases of the ASM from a subseasonal prediction perspective and provides evidence regarding the major contribution of internal atmospheric variability to the rapid development of biases. However, it is still unclear what aspects have caused the weakening Hadley cell and monsoon meridional circulation in the Asian monsoon region, although the over-produced convection over the equatorial Indian Ocean may lead to a weaker SASM (e.g. Jiang et al. 2012). Reasons for the sudden cooling of TP during the evolution of the monsoon are also unclear. Nevertheless, these biases may arise from the imperfection of initialization and the model itself. Initial shock may be an important factor of bias formation in coupled models (e.g., Zhang 2011), and this feature has been partially shown by our results which indicate that the precipitation in SASM region sometimes presents the strongest bias on the short-lead predictions. Also, the systematic biases are closely connected to model's performance (Turner et al. 2005; Lee et al. 2010). Hence, it is necessary to understand the formation and the impact of these biases from the point of view of predictability. The proportion of initial error and model deficiency to inaccuracy of prediction shows apparent spatial and temporal dependence (e.g., Drbohlav and Krishnamurthy 2010; Rai and Krishnamurthy 2011), which implies that further studies are needed to understand the spatial and temporal features about the relative contribution of unwell initialization and defective model to the biases.

It should be realized that prediction biases are always model dependent and our results are based only on the

hindcasts by CFSv2. Although suffered by some common problems such as representation of weak-than-observed Asian monsoon and unreasonable estimation of terrain-related precipitation, the predictions by CFSv2 still show apparent differences from the CFS version 1 (Yang et al. 2008a; Drbohlav and Krishnamurthy 2010), as well as from the ensemble average of state-of-the-art models (Lee et al. 2010; Rajeevan et al. 2012). The studies by Preethi et al. (2010) and Li et al. (2012) also revealed the model-to-model prediction biases of the Asian summer monsoon in EU projects DEMETER and ENSEMBLES. Moreover, the extent to which biases are dependent on lead time and the stage of monsoon evolution should also be different among models. Hence, understanding the formation and causes of biases based on multi-model predictions may be necessary in future studies.

Acknowledgments We thank the two anonymous reviewers for their valuable comments. This study was partially supported by the National Basic Research Program of China (973 Program: 2010CB951903), the National Natural Science Foundation of China (Grants 40905046 and 41105061), and the NOAA—China Meteorological Administration Bilateral Program.

References

Abhik S, Halder M, Mukhopadhyay P, Jiang X, Goswami BN (2012) A possible new mechanism for northward propagation of boreal summer intraseasonal oscillations based on TRMM and MERRA reanalysis. Clim Dyn. doi:10.1007/s00382-012-1425-x

Achuthavarier D, Krishnamurthy V (2010) Relation between intraseasonal and interannual variability of the South Asian monsoon in the National centers for environmental predictions forecast systems. J Geophys Res 115:D08104. doi:10.1029/2009JD012865

Barreiro M, Chang P (2004) A linear tendency correction technique for improving seasonal prediction of SST. Geophys Res Lett 31:L23209. doi:10.1029/2004GL021148

Bechtold P et al (2008) Advances in simulating atmospheric variability with the ECMWF model: from synoptic to decadal time-scales. Q J R Meteorol Soc 134:1337–1351

Chen D, Cane MA, Zebiak SE, Cañizares R, Kaplan A (2000) Bias correction of an ocean–atmosphere coupled model. Geophys Res Lett 27:2585–2588. doi:10.1029/1999GL011078

Drbohlav HKL, Krishnamurthy V (2010) Spatial structure, forecast errors, and predictability of the South Asian monsoon in CFS monthly retrospective forecasts. J Clim 23:4750–4769

Ek MB et al (2003) Implementation of Noah land surface model advances in the national centers for environmental prediction operational mesoscale eta model. J Geophys Res 108:8851. doi:10.1029/2002JD003296

Fu X, Wang B, Waliser DE, Tao L (2007) Impact of atmosphere-ocean coupling on the predictability of monsoon intraseasonal oscillations. J Atmos Sci 64:157–174

Fu X, Wang B, Bao Q, Liu P, Lee J (2009) Impacts of initial conditions on monsoon intraseasonal forecasting. Geophys Res Lett 36:L08801. doi:10.1029/2009GL037166

Fu X, Wang B, Lee J, Wang W, Gao L (2011) Sensitivity of dynamical intraseasonal prediction skills to different initial conditions. Mon Weather Rev 139:2572–2592

Gadgil S, Rajeevan M, Nanjundiah R (2005) Monsoon prediction—why yet another failure? Curr Sci 88:1389–1400

Goswami BN, Krishnamurthy V, Annamalai H (1999) A broad-scale circulation index for the interannual variability of the Indian summer monsoon. Q J R Meteorol Soc 125:611–633

Goswami BN, Wu G, Yasunari T (2006) The annual cycle, intraseasonal oscillations, and roadblock to seasonal predictability of the Asian summer monsoon. J Clim 19:5078–5099

Griffies SM, Harrison MJ, Pacanowsky RC, Rosati A (2003) A technical guide to MOM4. GFDL Ocean Group technical report 5, NOAA/GFDL, Princeton, NJ, 295 pp

Hoyos CD, Webster PJ (2007) The role of intraseasonal variability in the nature of Asian monsoon precipitation. J Clim 20:4402–4424

Jiang XA, Li T, Wang B (2004) Structures and mechanisms of the northward-propagating boreal summer intraseasonal oscillation. J Clim 17:1022–1039

Jiang XW, Yang S, Li Y, Kumar A, Liu X, Zuo Z, Jha B (2012) Seasonal-to-interannual prediction of the Asian summer monsoon in the NCEP climate forecast system Version 2. J Clim (conditionally accepted)

Kang IS et al (2002) Intercomparison of the climatological variations of Asian summer monsoon precipitation simulated by 10 GCMs. Clim Dyn 19:383–395

Krishnamurthy V, Shukla J (2008) Seasonal persistence and propagation of intraseasonal patterns over the Indian monsoon region. Clim Dyn 30:353–369

Krishnamurti TN, Subramaniam M, Daughenbaugh G, Oosterhof D, Xue JH (1992) One-month forecast of wet and dry spells of the monsoon. Mon Weather Rev 120:1191–1223

Krishnamurti TN, Mitra AK, Kumar TS, Yun WT, Dewar WK (2006) Seasonal climate forecasts of the South Asian monsoon using multiple coupled models. Tellus A 58:487–507

Lau NC, Nath MJ (2000) Impact of ENSO on the variability of the Asian–Australian monsoons as simulated in GCM experiments. J Clim 13:4287–4309

Lee JY et al (2010) How are seasonal prediction skills related to models' performance on mean state and annual cycle? Clim Dyn 35:267–283

Lee SS, Lee JY, Ha KJ, Wang B, Schemm JKE (2011) Deficiencies and possibilities for long-lead coupled climate prediction of the Western North Pacific–East Asian summer monsoon. Clim Dyn 36:1173–1188

Li C, Lu R, Dong B (2012) Predictability of the western North Pacific summer climate demonstrated by the coupled models of ENSEMBLES. Clim Dyn 39:329–346

Liang J, Yang S, Hu Z, Huang B, Kumar A, Zhang Z (2009) Predictable patterns of Asian and Indo-Pacific summer precipitation in the NCEP CFS. Clim Dyn 32:989–1001

Lin JL et al (2008) Subseasonal variability associated with Asian summer monsoon simulated by 14 IPCC AR4 coupled GCMs. J Clim 21:4541–4567

Misra V (2008) Coupled interactions of the monsoons. Geophys Res Lett 35:L12705. doi:10.1029/2008GL033562

Moorthi S, Pan HL, Caplan P (2001) Changes to the 2001 NCEP operational MRF/AVN global analysis/forecast system. NWS Tech 484. Available at http://www.nws.noaa.gov/om/tpb/484.htm

Pope VD, Stratton RA (2002) The processes governing horizontal resolution sensitivity in a climate model. Clim Dyn 19:211–236

Preethi B, Kripalani RH, Krishna Kumar K (2010) Indian summer monsoon rainfall variability in global ocean-atmospheric models. Clim Dyn 35:1521–1533

Rai S, Krishnamurthy V (2011) Error growth in climate forecast system daily retrospective forecasts of South Asian monsoon. J Geophys Res 116:D03108. doi:10.1029/2010JD014840

Rajeevan M, Unnikrishnan CK, Preethi B (2012) Evaluation of the ENSEMBLES multi-model seasonal forecasts of Indian summer monsoon variability. Clim Dyn 38:2257–2274

Saha S et al (2006) The NCEP climate forecast system. J Clim 19:3483–3517

Saha S et al (2010) The NCEP climate forecast system reanalysis. Bull Am Meteorol Soc 91:1015–1057

Sengupta D, Goswami BN, Senan R (2001) Coherent intraseasonal oscillations of ocean and atmosphere during the Asian summer monsoon. Geophys Res Lett 28:4127–4130

Sperber KR, Hameed S, Potter GL, Boyle JS (1994) Simulation of the northern summer monsoon in the ECMWF model: sensitivity to horizontal resolution. Mon Weather Rev 122:2461–2481

Sperber KR, Palmer TN (1996) Interannual tropical rainfall variability in general circulation model simulations associated with the Atmospheric Model Intercomparison Project. J Clim 9:2727–2750

Turner AG, Inness PM, Slingo JM (2005) The role of the basic state in the ENSO–monsoon relationship and implications for predictability. Q J R Meteorol Soc 131:781–804

Wang B (2006) The Asian monsoon. Praxis Publishing, Chichester

Wang B, Wu R, Li T (2003) Atmosphere–warm ocean interaction and its impacts on Asian–Australian monsoon variation. J Clim 16:1195–1211

Wang B, Kang IS, Lee JY (2004) Ensemble simulations of Asian–Australian monsoon variability by 11 AGCMs. J Clim 17:803–818

Wang B, Ding QH, Fu XH, Kang IS, Jin K, Shukla J, Doblas-Reyes F (2005) Fundamental challenge in simulation and prediction of summer monsoon rainfall. Geophys Res Lett 32:L15711. doi: 10.1029/2005GL022734

Wang B et al (2008) How accurately do coupled climate models predict the leading modes of Asian–Australian monsoon interannual variability? Clim Dyn 30:605–619

Wang W, Chen M, Kumar A (2009) Impacts of ocean surface on the northward propagation of the boreal-summer intraseasonal oscillation in the NCEP climate forecast system. J Clim 22:6561–6576

Wang W, Xie P, Yoo SH, Xue Y, Kumar A, Wu X (2010) An assessment of the surface climate in the NCEP climate forecast system reanalysis. Clim Dyn 37:1601–1620

Weaver SJ, Wang W, Chen M, Kumar A (2011) Representation of MJO variability in the NCEP Climate Forecast System. J Clim 24:4676–4694

Webster PJ, Yang S (1992) Monsoon and ENSO: selectively interactive systems. Q J R Meteorol Soc 118:877–926

Wen M, Yang S, Vintzileos A, Higgins W, Zhang R (2012) Impacts of model resolutions and initial conditions on predictions of the Asian summer monsoon by the NCEP climate forecast system. Weather Forecasting 27:629–646

Wu R, Kirtman B (2005) Roles of Indian and Pacific Ocean air–sea coupling in tropical atmospheric variability. Clim Dyn 25:155–170

Xie P, Arkin PA (1997) Global precipitation: a 17-year monthly analysis based on gauge observations, satellite estimates, and numerical model outputs. Bull Am Meteorol Soc 78:2539–2558

Xue Y, Huang B, Hu ZZ, Kumar A, Wen C, Behringer D, Nadiga S (2010) An assessment of oceanic variability in the NCEP climate forecast system reanalysis. Clim Dyn 37:2511–2539

Yang S, Zhang Z, Kousky VE, Higgins RW, Yoo SH, Liang J, Fan Y (2008a) Simulations and seasonal prediction of the Asian summer monsoon in the NCEP climate forecast system. J Clim 21:3755–3775

Yang S, Wen M, Higgins RW (2008b) Sub-seasonal features of the Asian summer monsoon in the NCEP climate forecast system. ACTA Oceanol Sin 27:88–103

Yang S, Wen M, Yang R, Higgins W, Zhang R (2011) Impacts of land process on the onset and evolution of Asian summer monsoon in the NCEP climate forecast system. Adv Atmos Sci 28:1301–1317

Yhang YB, Hong SY (2008) Improved physical processes in a regional climate model and their impact on the simulated summer monsoon circulations over East Asia. J Clim 21:963–979

Zhang S (2011) A study of impacts of coupled model initial shocks and state–parameter optimization on climate predictions using a simple pycnocline prediction model. J Clim 24:6210–6226